

# Redshifted 21cm Observations of High Redshift Quasar Proximity Zones

J. Stuart B. Wyithe

*School of Physics, University of Melbourne, Parkville, Victoria, Australia*  
 Email: [swyithe@unimelb.edu.au](mailto:swyithe@unimelb.edu.au)

12 August 2021

## ABSTRACT

The introduction of low-frequency radio arrays is expected to revolutionize the study of the reionization epoch. Observation of the contrast in redshifted 21cm emission between a large HII region and the surrounding neutral intergalactic medium (IGM) will be the simplest and most easily interpreted signature. However the highest redshift quasars known are thought to reside in an ionized IGM. Using a semi-analytic model we describe the redshifted 21cm signal from the IGM surrounding quasars discovered using the *i*-drop out technique (i.e. quasars at  $z \sim 6$ ). We argue that while quasars at  $z < 6.5$  seem to reside in the post overlap IGM, they will still provide valuable probes of the late stages of the overlap era because the light-travel time across a quasar proximity zone should be comparable to the duration of overlap. For redshifted 21cm observations within a 32MHz bandpass, we find that the subtraction of a spectrally smooth foreground will not remove spectral features due to the proximity zone. These features could be used to measure the neutral hydrogen content of the IGM during the late stages of reionization. The density of quasars at  $z \sim 6$  is now well constrained. We use the measured quasar luminosity function to estimate the prospects for discovery of high redshift quasars in fields that will be observed by the Murchison Widefield Array.

**Key words:** cosmology; diffuse radiation, large scale structure, theory – galaxies; high redshift, intergalactic medium

## 1 INTRODUCTION

The reionization of cosmic hydrogen by the first stars and quasars (e.g. Barkana & Loeb 2001), was an important milestone in the history of the Universe. The recent discovery of distant quasars has allowed detailed absorption studies of the state of the high redshift intergalactic medium (IGM) at a time when the universe was less than a billion years old (Fan et al. 2006; White et al. 2003). Several studies have used the evolution of the ionizing background inferred from these spectra to argue that the reionization of cosmic hydrogen was completed just beyond  $z \sim 6$  (Fan et al. 2006; Gnedin & Fan 2006; White et al. 2003). However, other authors have claimed that the evidence for this rapid change becomes significantly weaker for a different choice of density distribution in the IGM (Becker et al. 2007). Different arguments in favour of a rapidly evolving IGM at  $z > 6$  are based on the properties of the putative HII regions inferred around the highest redshift quasars (Wyithe & Loeb 2004; Wyithe, Loeb, & Carilli 2005; Mesinger & Haiman 2005). However, Bolton & Haehnelt (2007a) and Lidz et al. (2007)

have demonstrated that the interpretation of the spectral features is uncertain and that the observed spectra could either be produced by an HII region, or by a classical proximity zone. One reason for the ambiguity in interpreting these absorption spectra is that  $\text{Ly}\alpha$  absorption can only be used to probe neutral fractions that are smaller than  $10^{-3}$  owing to the large cross-section of the  $\text{Ly}\alpha$  resonance. Thus studies of the IGM in  $\text{Ly}\alpha$  absorption become inconclusive in the era of interest for reionization.

On the other hand there is mounting evidence that the reionization of the IGM was photon starved. Firstly Bolton & Haehnelt (2007b) have shown that the observed ionization rate at  $z \lesssim 6$  implies an emissivity that is only just sufficient to have reionized the universe by that time. Similarly, the small escape fractions found for high redshift galaxies by several studies (Chen et al. 2007; Gnedin et al. 2007; Srbinovsky & Wyithe 2008) together with the star formation rates implied by the observed high redshift galaxy population suggest a photon budget that struggles to have been sufficient to reionize the universe by  $z \sim 6$  (Gnedin 2007; Srbinovsky & Wyithe 2008). These results imply that while

the IGM seems to be highly ionized along the lines-of-sight towards the highest redshift quasars discovered in current surveys, the reionization epoch cannot be at a substantially higher redshift unless the emissivity grows significantly at  $z > 6$ . Indeed this outcome may be suggested by the large optical depth to electron scattering measured by the WMAP satellite (Spergel et al. 2007).

A better probe of the process of reionization will be provided by redshifted 21cm observations. Reionization starts with ionized (HII) regions around galaxies, which later grow to surround groups of galaxies. The process of reionization is completed when these HII regions overlap (defining the so-called *overlap* epoch) and fill-up most of the volume between galaxies. Several probes of the reionization epoch in redshifted 21cm emission have been suggested in a large body of literature. These include observation of 21cm emission as a function of redshift averaged over a large area of the sky. This provides a direct probe of the evolution in the neutral fraction of the IGM, the so-called global step (Shaver, Windhorst, Madau & de Bruyn 1999; Gnedin & Shaver 2004). A more powerful probe will be provided by observation of the power-spectrum of fluctuations together with its evolution with redshift. This observation would trace the evolution of neutral gas with redshift as well as the topology of the reionization process (e.g. Tozzi, Madau, Meiksin & Rees 2000; Furlanetto, Hernquist & Zaldarriaga 2004; Loeb & Zaldarriaga 2004; Barkana & Loeb 2005a,b,c). It is thought that the amplitude of 21cm fluctuations will be greatest when the neutral fraction in the IGM is around 50% (Furlanetto et al. 2004; Lidz et al. 2007). Thus, while the power-spectrum should prove to be the best technique for study of the bulk of the reionization epoch, it may not be a sensitive probe of the very late stages of the overlap era.

Finally, observations of individual quasar HII regions will probe quasar physics as well as the evolution of the neutral gas in the surrounding IGM (Wyithe & Loeb 2004b; Kohler, Gnedin, Miralda-Escude & Shaver 2005). Kohler et al. (2005) have generated synthetic spectra using cosmological simulations. They conclude that quasar HII regions will provide the most prominent individual cosmological signals. These individual signatures will be most readily detected a-posteriori, around known high redshift quasars (Wyithe, Loeb & Barnes 2005; Geil & Wyithe 2007). These studies have focused on the scenario of a quasar expanding into a significantly neutral IGM. However the density of quasars is very low at high redshift, while as discussed above, the IGM allows substantial Ly $\alpha$  transmission and so is thought to be highly ionized along the lines-of-sight to nearly all of the known high redshift quasars.

The conventional wisdom has been that the 21cm signal disappears after the *overlap* epoch is complete, because there is little neutral hydrogen left through most of intergalactic space. However observations of damped Ly $\alpha$  systems out to a redshift of  $z \sim 4$  show the cosmological density parameter of HI to be  $\Omega_{\text{HI}} \sim 10^{-3}$  (Prochaska et al. 2005). In the standard cosmological model the density parameter of baryons is  $\Omega_{\text{b}} \sim 0.04$ , so that the mass-averaged neutral hydrogen fraction at  $z \sim 4$  (long after the end of the HII overlap epoch) is  $F_{\text{m}} \sim 0.03$ . This neutral gas does not contribute significantly to the effective Ly $\alpha$  optical depth, which is sensitive to the volume averaged neutral fraction (with a value that is orders of magnitude lower). However the redshifted

21cm emission is sensitive to the total (mass-weighted) optical depth of this neutral gas. Observations of the redshifted 21cm signal would therefore detect the total neutral hydrogen content in a volume of IGM dictated by the observatory beam and frequency band-pass (Wyithe & Loeb 2007). Since quasars could be observed through the entire overlap epoch, redshifted 21cm observations of the surrounding IGM could provide a bridge between 21cm fluctuations at high redshift and the well studied techniques utilizing the Ly $\alpha$  forest following the completion of reionization.

We begin by describing our density dependent semi-analytic model for the reionization history (§ 2). We next describe our calculation of the depletion of neutral hydrogen near the vicinity of a high redshift quasar (§ 3). Then in § 4 and § 5 we describe the 21cm signal from the proximity zones and estimate of the effect of foreground removal. Finally we summarize existing observations of the high redshift quasar luminosity function (§ 6), and predict the number that will be found in future surveys (§ 7) before presenting our conclusions in § 8. Throughout the paper we adopt the set of cosmological parameters determined by WMAP (Spergel et al. 2007) for a flat  $\Lambda$ CDM universe, namely  $\Omega_{\text{m}} = 0.24$ ,  $\Omega_{\Lambda} = 0.76$  and  $h = 0.73$ . In computation of the mass function we assume a primordial power spectrum defined by a power law with index  $n = 0.95$ , an exact transfer function given by Bardeen et al. (1986) and rms mass density fluctuations with a sphere of radius  $R_{\text{s}} = 8h^{-1}\text{Mpc}$  of  $\sigma_{\text{s}} = 0.76$ .

## 2 SEMI-ANALYTIC MODEL FOR THE REIONIZATION HISTORY

In this section we describe the semi-analytic model which we use to describe the ionization state of the IGM during the reionization history of the IGM. Our model is based on the work of Miralda-Escude et al. (2000) who presented a prescription which allows the calculation of an effective recombination rate in an inhomogeneous universe by assuming a maximum over density ( $\Delta_{\text{c}}$ ) penetrated by ionizing photons within HII regions. The model assumes that reionization progresses rapidly through islands of lower density prior to the overlap of individual cosmological ionized regions. Following the overlap epoch, the remaining regions of high density are gradually ionized. It is therefore hypothesized that at any time, regions with gas below some critical over density  $\Delta_{\text{i}} \equiv \rho_{\text{i}}/\langle\rho\rangle$  are highly ionized while regions of higher density are not. In what follows, we draw primarily from their prescription and refer the reader to the original paper for a detailed discussion of its motivations and assumptions. Wyithe & Loeb (2003) employed this prescription within a semi-analytic model of reionization. This model was extended by Srbinsky & Wyithe (2007) and by Wyithe, Bolton & Haehnelt (2007). We summarise the model in the remainder of this section, but refer the reader to those papers for a full description.

Within the model of Miralda-Escude et al. (2000) we describe the post-overlap evolution of the IGM by computing the evolution of the fraction of mass in regions with over density below  $\Delta_{\text{i}}$ ,

$$F_{\text{M}}(\Delta_{\text{i}}) = \int_0^{\Delta_{\text{i}}} d\Delta P_{\text{V}}(\Delta)\Delta, \quad (1)$$

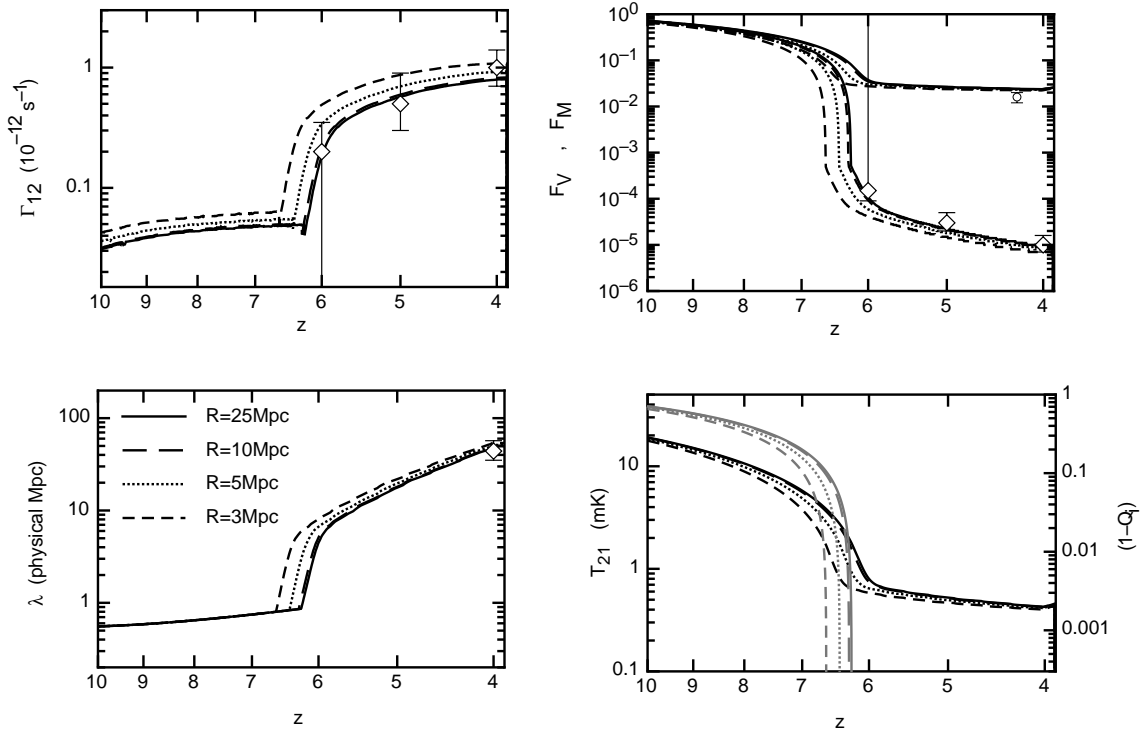


**Figure 1.** The effect of over density on the redshift of overlap, and the subsequent ionization state of the IGM. Five cases are shown, corresponding to over densities evaluated within spheres with radii of 3, 5, 10 and 25 physical Mpc, centered on a quasar host of mass  $M = 10^{13} M_{\odot}$  at  $z \sim 6$ . In each case we evaluate the reionization history assuming the mean over density surrounding the quasar. *Upper Left Panel:* The ionization rate as a function of redshift. The observational points are from Bolton et al. (2007b). *Upper Right Panel:* The volume (lower curves) and mass (upper curves) averaged fractions of neutral gas in the universe. Also shown (dotted lines) is the fraction of the IGM yet to overlap ( $1 - Q_i$ ). The observational points for the volume averaged neutral fraction are from Bolton et al. (2007b), while the observed mass-fractions are from the damped Ly $\alpha$  measurements of Prochaska et al. (2005). *Lower Left Panel:* The mean-free-path for ionizing photons computed using the formalism in § 2. The data points are based on Storrie-Lombardi et al. (1994). *Lower Right Panel:* The evolution of the mean 21cm brightness temperature (in mK) with redshift (solid lines). For comparison, the fraction of IGM yet to overlap ( $1 - Q_i$ ) is over plotted.

where  $P_V(\Delta)$  is the volume weighted probability distribution for  $\Delta$ . Miralda-Escude et al. (2000) quote a fitting function which provides a good fit to the volume weighted probability distribution for the baryon density in cosmological hydrodynamical simulations. This probability distribution remains a reasonable description at high redshift when confronted with a more modern cosmology and updated simulations, although the addition of an analytical approximation for the high density tail of the distribution remains necessary as a best guess at correcting for numerical resolution (Bolton & Haehnelt 2007b).

In the post overlap era the model computes the evolution of  $\Delta_i$ . In the pre-overlap era we define the quantity  $Q_i$  to be the volume filling factor within which all matter at densities below  $\Delta_i$  has been ionized. Within this formalism, the epoch of overlap is precisely defined as the time when  $Q_i$  reaches unity. However, prior to overlap we have only a single equation to describe the evolution of two independent quantities  $Q_i$  and  $F_M$  (or equivalently  $\Delta_i$ ). The relative growth of these depends on the luminosity function and spatial distribution of the sources. In our model we follow Miralda-Escude et al. (2000) and assume  $\Delta_i$  to

be constant<sup>1</sup> (of value  $\Delta_c$ ) with redshift before the overlap epoch, and in this paper compute results for models that assume  $\Delta_c = 20$ . Our approach is to compute a reionization history given a particular value of  $\Delta_c$ , combined with assumed values for the efficiency of star-formation and the fraction of ionizing photons that escape from galaxies. With this history in place we then compute the evolution of the background radiation field due to these same sources. After the overlap epoch, ionizing photons will experience attenuation due to residual over dense pockets of HI gas. We use the description of Miralda-Escude et al. (2000) to estimate the ionizing photon mean-free-path, and subsequently derive the

<sup>1</sup> We note that the assumption of a fixed value of  $\Delta_c$  (and hence a slowly evolving mean-free-path) in the pre overlap era is artificial. Indeed,  $\Delta_c$  is probably only a meaningful quantity after overlap is complete and the mean-free-path is set by dense systems, while before overlap the mean-free-path is sensitive to the size of HII regions (which increases with redshift). However, within the model of Miralda-Escude et al. (2000), the value of  $\Delta_c$  and the ionization fraction are both unknowns prior to overlap, with only one equation to govern their evolution. An assumption regarding  $\Delta_c$  is therefore unavoidable within the formalism used in this paper.

attenuation of ionizing photons. We then compute the flux at the Lyman-limit in the IGM due to sources immediate to each epoch, in addition to redshifted contributions from earlier epochs.

We assume the spectral energy distribution (SED) of population-II star forming galaxies with a gas metallicity of 0.05 and a Scalo IMF, using the model presented in Leitherer et al. (1999). The star formation rate per unit volume is computed based on the collapsed fraction obtained from the extended Press-Schechter (1974) model (Bond et al. 1991) in halos above the minimum halo mass for star formation, together with an assumed star formation efficiency ( $f_*$ ). In a cold neutral IGM beyond the redshift of reionization, the collapsed fraction should be computed for halos of sufficient mass to initiate star formation. The critical virial temperature is set by the temperature ( $T_N \sim 10^4$  K) above which efficient atomic hydrogen cooling promotes star formation. Following the reionization of a region, the Jeans mass in the heated IGM limits accretion to halos above  $T_1 \sim 10^5$  K (Efstathiou 1992; Thoul & Weinberg 1996; Dijkstra et al. 2004). Only a fraction of ionizing photons produced by stars enter the IGM. Therefore an additional factor of  $f_{\text{esc}}$  (the escape fraction) must be included when computing the emissivity of galaxies. In our fiducial model we assume this escape fraction to be independent of mass. We define a parameter  $f_{*,\text{esc}} \equiv f_* f_{\text{esc}}$ .

Figure 1 shows models for the reionization of the IGM and the subsequent post-overlap evolution of the ionizing radiation field. The fiducial model (shown by the thick grey curves) has  $f_{*,\text{esc}} = 0.00375$ . Our model allows the bias of reionization near a massive halo to be included explicitly, and we show histories corresponding to regions within  $R = 3, 5, 10$  and  $25$  proper Mpc surrounding a quasar host of mass  $M = 10^{13} M_\odot$ . In the top left panel of Figure 1 we show the evolution of the ionization rate. The observational points are from the simulations of Bolton et al. (2007b; based on the observations of Fan et al. 2006). In the upper-right panels we plot the corresponding volume and mass (upper curves) averaged fractions of neutral gas in the universe. The observational points for the volume averaged neutral fraction are from Bolton et al. (2007b), while the observed mass-fractions are from the damped Ly $\alpha$  measurements of Prochaska et al. (2005), and therefore represent lower limits on the total HI content of the IGM. Both curves show excellent agreement with these quantities, despite their differing by 3 orders of magnitude. In computing the volume averaged neutral fraction we have followed standard practice and assumed ionization equilibrium with an ionizing background at all over densities. However in an IGM that includes dense regions that are self-shielded, this value under estimates the true value. We note that the inclusion of fully neutral gas at densities above the self shielding over density does not modify the predicted value of effective Ly $\alpha$  transmission, from which IGM properties are inferred. However neutral hydrogen above the self-shielding threshold does contribute significantly to the volume averaged neutral fraction (in addition of course to the mass averaged neutral fraction) interpreted from Ly $\alpha$  absorption spectra.

In the lower-left panel we plot the evolution of the ionizing photon mean-free-path. The data points are based on Storrie-Lombardi et al. (1994). Again the model is in good agreement with the available observations. We note that the

observed mean-free-path is found from the number density of Ly-limit systems and is independent of the Ly $\alpha$  forest absorption derived quantities of ionization rate and volume averaged neutral fraction, as well as being independent of the HI mass-density measurements. Our simple model therefore simultaneously reproduces the evolution of three independent measured quantities. In the lower-right panel we plot the corresponding evolution of the 21cm brightness temperature (dark lines). The grey lines show the evolution of the filling factor of ionized regions ( $1 - Q_i$ ).

### 3 QUASAR PROXIMITY ZONES DURING OVERLAP

The enhanced ionization rate near quasars at moderate redshift produces a region of thinned Ly $\alpha$  forest that extends for several Mpc (e.g. Scott et al. 2000). This thinning of the Ly $\alpha$  forest is termed the proximity effect and the region of enhanced ionization the proximity zone. Prior to the end of reionization the proximity zone is not defined since there is no ionizing background and instead the quasar contributes to an enlarged, distinct HII region. In this section we aim to model the effect of the quasar flux on the mass averaged neutral fraction within the proximity zones of quasars during the overlap era.

Our semi-analytic model provides a framework within which to model the depletion of neutral hydrogen within the proximity zone. Since gas is neutral at over densities above  $\Delta_i$ , we must estimate the change in  $\Delta_i$  induced by the quasar. We begin with the ionization rate from our semi-analytic model as a function of radius from the quasar host. We then add the ionization rate due to a quasar with luminosity of  $0.7 \times 10^{57} \text{s}^{-1}$ , which corresponds to a quasar with an absolute luminosity that is around a magnitude fainter than the most luminous SDSS  $z \sim 6$  quasars. This process includes calculation of biased reionization within the vicinity of the quasar host, but does not include the increase in ionizing photon mean-free-path that would result from the presence of quasar flux. We therefore underestimate the ionization rate in the vicinity of the quasar. The most over dense regions of the IGM are self shielding to ionizing radiation. The over density of a clump at which gas becomes self shielding may be estimated from (Furlanetto & Oh 2005; Bolton & Haehnelt 2007b)

$$\Delta_{\text{SSC}} = 50N \left( \frac{1+z}{7} \right)^{-3} \Gamma_{12}^{2/3}, \quad (2)$$

where we have neglected the mild dependence on temperature. This expression assumes that the typical size of an absorber with over density  $\Delta$  is the local Jeans length, and that the absorber becomes optically thick to Lyman limit photons when the column density  $N_{\text{HI}}$  exceeds  $N\sigma_{\text{HI}}^{-1}$ , where  $\sigma_{\text{HI}}$  is the hydrogen photo-ionization cross-section at the Lyman limit. The coefficient  $N$  has been previously assumed to equal unity, but is somewhat arbitrary, and we discuss its value below.

Our model for the reionization of the IGM surrounding a quasar is not internally consistent, which would require a full numerical simulation. On the other hand, such a simulation is currently beyond the available numerical resolution over volumes sufficiently large to host a high redshift quasar

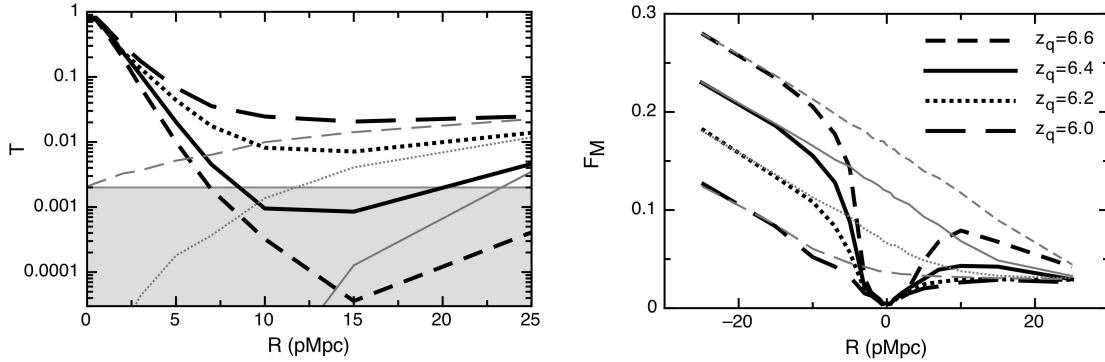


**Figure 2.** Impact of the quasar flux on local IGM properties. *Left:*  $\text{Ly}\alpha$  transmission as a function of distance from the quasar in units of proper Mpc (dark curves). The shaded region shows the limit on transmission in the Gunn-Peterson troughs of the deepest available spectra. *Right:* Mass weighted neutral fraction as a function of distance from the quasar (dark curves). In each panel examples are shown corresponding to 4 different quasar redshifts. Also shown are the corresponding examples for the mean IGM, centered on the assumed quasar redshifts (grey curves).

proximity zone, while the damped  $\text{Ly}\alpha$  systems thought to dominate the high redshift neutral gas are currently subject to many model uncertainties (Nagamine et al. 2007). The inconsistency within our model can be traced partly to the fact that  $\Delta_i$  is computed in a non-equilibrium condition as reionization progresses, while  $\Delta_{\text{SSC}}$  is computed in ionization equilibrium with an estimate of the ionizing flux. However most importantly, one has to assume a density profile in order to calculate a column density. The density profiles which are assumed in the distribution  $P_V(\Delta)$  differ from the top-hat density profile assumed in calculation of  $\Delta_{\text{SSC}}$  (Furlanetto & Oh 2005). In order to make the model internally consistent we therefore choose the value of  $N$  in equation (2) at each redshift such that  $\Delta_{\text{SSC}} = \Delta_i$  in the mean ionizing background<sup>2</sup> (i.e. far from the quasar). The mass averaged neutral fraction within the proximity zone at a radius  $R$  is then obtained from

$$F_M(R) = \int_0^{\Delta_{\text{SSC}}} d\Delta \Delta P_V(\Delta) x_{\text{HI}}, \quad (3)$$

where  $x_{\text{HI}}$  is the neutral fraction of hydrogen, which is evaluated assuming ionization equilibrium at overdensities  $\Delta < \Delta_{\text{SSC}}$ , and is equal to unity when  $\Delta > \Delta_{\text{SSC}}$ .

An important ingredient in our modeling is the computation of the local ionization rate at the retarded time along the line of sight. The use of retarded time is particularly important for quasars observed near the end of reionization since the ionization state of the IGM changes dramatically during the light travel time of a quasar proximity zone. In regions of the IGM observed in front of the quasar (i.e. at lower redshift) we assume ionization equilibrium of the hydrogen with the sum of quasar and ionizing background flux at all radii. This is because the IGM is observed in photons that arrive at the observer at the same time as photons emitted by the quasar (either when observed in absorption against the quasar, or in 21cm emission). However the 21cm emission from IGM behind the quasar can only be subject

to ionization by quasar flux if it is located within a distance  $R = ct_q/2$  of the quasar (where  $t_q$  is the quasar lifetime).

The resulting model proximity zones, described by the mass averaged neutral fraction as a function of distance from the quasar (dark curves) are plotted in the right-hand panel of Figure 2. Since the neutral gas is confined to discrete clumps following reionization, an individual line of sight through a proximity zone will not have a smooth profile in neutral hydrogen density. However our semi-analytic model is unable to compute individual realizations of the IGM, but rather computes the average behaviour which is represented by a smooth profile. Thus, examples of these smooth profiles are shown corresponding to 4 different quasar redshifts which cover the end of the overlap epoch (as predicted within our model). The curves show a proximity zone extending to around 10 proper Mpc. The curves also show an asymmetry in the proximity zone, which has a greater contrast behind the quasar. This asymmetry is largest earlier in the overlap era. Also shown for comparison are the corresponding examples for the mean IGM, centered on the assumed quasar redshifts (grey curves).

We also compute the  $\text{Ly}\alpha$  transmission as a function of distance from the quasar, and plot the results in the left-hand panel of Figure 2. These transmission curves may be compared with observations of high redshift quasars. The deepest spectra of high redshift quasars reach a limit of  $T \sim 0.002$  towards quasars at  $z \sim 6.3-6.4$ . This limit is shaded grey. Our model predicts that the Gunn-Peterson Trough will appear in the spectra of quasars at  $z \sim 6.4$  (in agreement with observation), even though the IGM is highly ionized. The model Gunn-Peterson trough begins at a distance of approximately 7-8Mpc from the quasar and extends for  $\sim 10$ Mpc. The corresponding examples of transmission for the mean IGM, centered on the assumed quasar redshifts are plotted for comparison (grey curves). In this example the quasar has little impact on the redshift at which the Gunn-Peterson trough would appear, since the onset is at a large distance from the quasar.

In the left hand panel of Figure 3 we plot the mass weighted neutral fraction as a function of redshift. The results of our modeling for the mass fraction in the vicinity of

<sup>2</sup> The modification of the value  $N$  in this process could be thought of as providing a correction that accounts for the effect of the density profile on the column density.

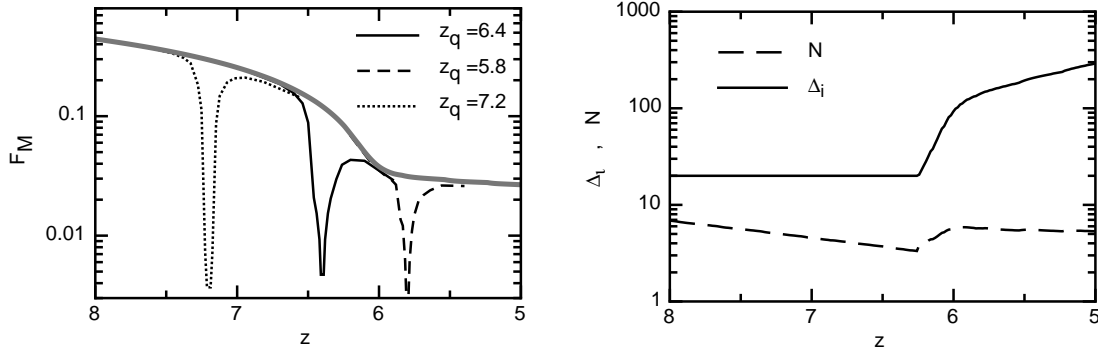


**Figure 3.** *Left:* Mass weighted neutral fraction as a function of redshift. The evolution for the mean IGM with redshift is shown as the grey line. The results of our modeling for the mass fraction in the vicinity of a quasar are shown as the dark curves for quasars at three different redshifts. *Right:* The evolution of  $\Delta_i$  and  $N$  as a function of redshift.

a quasar are shown as the dark curves for quasars at three different redshifts. For comparison the evolution of the mean IGM with redshift is shown as the grey line. On the right hand side we show the value of the pre factor  $N$  in equation (2) for  $\Delta_{SSC}$ , as well as  $\Delta_i$ . Our model has  $N \sim 4$  for most of the redshift range of interest, and shows that while it is not constant,  $N$  evolves much more slowly than  $\Delta_i$ . Before proceeding, we note that the quantitative predictions of our model will be sensitive to the applicability of the assumed distribution of over densities  $P_V(\Delta)$ , which is not directly measured in numerical simulations (Bolton & Haehnelt 2007b).

#### 4 21CM OBSERVATIONS OF QUASAR PROXIMITY ZONES

We next estimate the 21cm signal corresponding to the proximity zones described in the previous section. The 21cm brightness temperature contrast corresponding to IGM at the mean density is

$$T(R) = 22\text{mK} \left( \frac{1+z}{7.5} \right)^{1/2} (1 - Q_i F_M(\Delta_i, R)). \quad (4)$$

The resulting 21cm brightness temperature profiles as a function of observed frequency are shown in Figure 4 (dark lines). For a quasar at  $z \sim 6.6$  the model predicts that the expected contrast in front of the quasar is only  $\sim 1\text{mK}$ , while at redshifts beyond the quasar the contrast would be as large as  $5\text{mK}$ . On the other hand, around a quasar at  $z \sim 6.0$  the contrast would only be  $\sim 0.5 - 1\text{mK}$ . Also shown for comparison are the corresponding examples for the mean IGM, centered on the assumed quasar redshifts (grey curves).

We estimate the uncertainty for observations using the configuration of the Murchison Widefield Array (MWA<sup>3</sup>), which is currently under construction and will comprise a phased array of 500 tiles (each tile will contain 16 cross-dipoles) distributed over an area with diameter 1.5km. The uncertainty was computed assuming 1000 hours of observing time. When forming a map from the available visibilities it is assumed that resolution has been compromised for lower

noise in the image by choosing a maximum baseline to be included (Geil & Wyithe 2007). We chose a synthesised beam (full beam width at half maximum) of  $\theta_{\text{beam}} = 3.2'$ <sup>4</sup> which would be appropriate for quasar proximity zones. The thermal noise corresponding to this angular scale for the MWA is (Geil & Wyithe 2007)

$$\Delta T = 17\text{mK} \left( \frac{1+z}{8.65} \right)^{2.6} \left( \frac{\Delta\nu}{0.07\text{MHz}} \right)^{-0.5} \left( \frac{t_{\text{int}}}{100\text{hr}} \right)^{-0.5}, \quad (5)$$

where  $\Delta\nu$  is the width of the frequency bin and  $t_{\text{int}}$  is the integration time. At  $z \geq 6.4$ , the error bars shown correspond to an observation of a single quasar, while at  $z = 6.2$  and  $z = 6.0$  the errors refer to the average signal from stacks of 3 and 10 quasars respectively. These numbers are motivated by the expected number counts in planned surveys and will be discussed in § 7. The sizes of the error bars correspond to binning over the interval in between the points shown (so that the errors would be independent). The proximity zones would be detectable with good significance in the scenario described.

We have computed line-of-sight 21cm spectra, while observations will be made at finite resolution. In the case of spherical proximity zones, finite resolution will introduce smoothing across the boundaries in observed 21cm spectra. For this reason we have restricted our analysis to spectra measured within a single synthesised beam centered on the quasar line-of-sight. If the proximity zone were spherical, the transverse size of the synthesised beam ( $\theta_{\text{beam}} = 3.2'$ ) at the edge of the proximity zone would subtend  $\sim 20$  degrees, making the smoothing negligible. Of course the proximity zone is unlikely to be spherical. Suppose that the quasar were beamed with an opening angle  $\alpha$ . If the transverse extent of the synthesised beam were wider than the emission region at the edge of the proximity zone, we would again expect smoothing of the boundary in the observed 21cm spectrum. However, given  $\theta_{\text{beam}} = 3.2'$ , the above argument implies that the spectrum should not be subject to smoothing so long as  $\alpha \gtrsim 20$  degrees (unless the quasar beaming is misaligned with the line of sight by  $\sim \alpha$ ).

<sup>3</sup> see <http://www.haystack.mit.edu/ast/arrays/mwa/index.html>

<sup>4</sup> This corresponds to 5.5' central peak to first null, which is often quoted as the resolution.

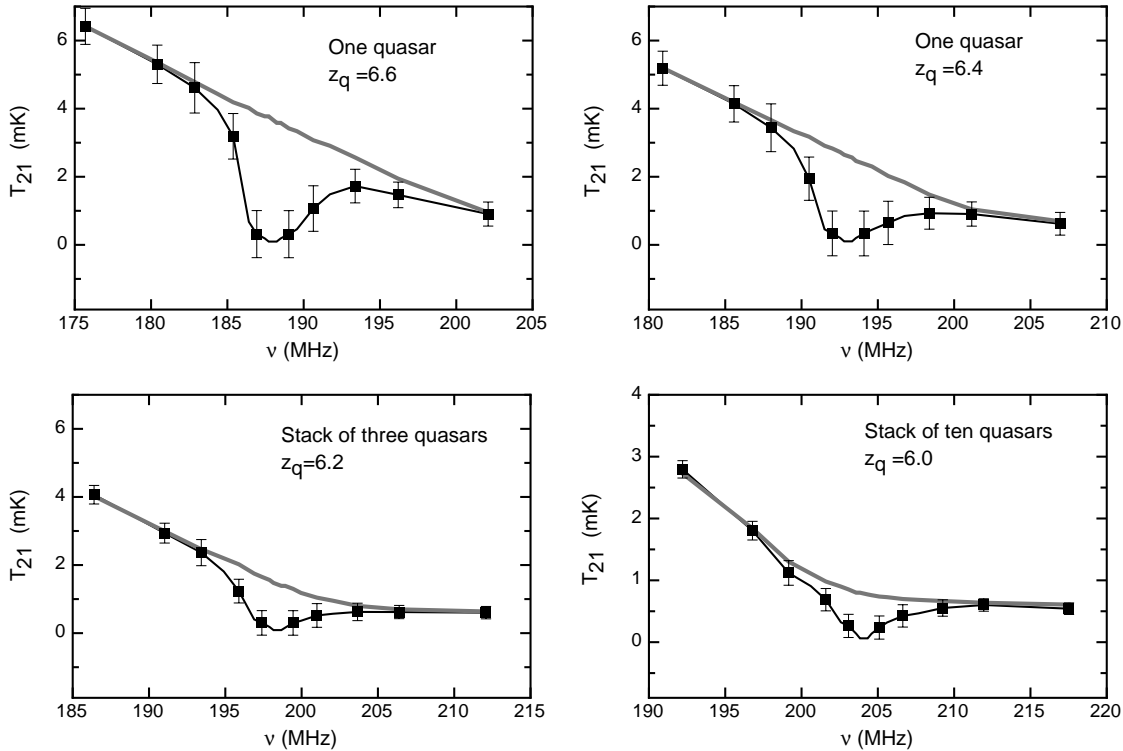


**Figure 4.** The 21cm brightness temperature as a function of observed frequency. The four panels show examples corresponding to 4 different quasar redshifts. Also shown are the corresponding examples for the mean IGM, centered on the assumed quasar redshifts (grey curves). At  $z \geq 6.4$ , the error bars shown correspond to an observation of 1000 hours with the MWA using a maximum baseline corresponding to a  $3.2'$  beam. At  $z = 6.2$  and  $z = 6.0$  the errors assume an average signal from stacks of 3 and 10 quasars respectively.

Furthermore, in the examples shown at  $z \leq 6.2$  we have assumed that the spectra from several quasars with the same luminosity and redshift could be stacked. In practice this process would be subject to several complications. First, the high redshift edge of the QSO proximity zone may lie in the pre-overlap era. In this case we would expect significant variation between quasars owing to the patchiness of reionization. In addition, the separation in redshift of the quasars available might exceed the depth of the proximity zones. Combining the spectra of different quasars in order to increase signal-to-noise would therefore be non-trivial.

Following the completion of overlap in a region of IGM the neutral gas is in a collection of dense pockets rather than being diffusely distributed in the IGM. There is therefore an additional component of uncertainty for the spectra shown in Figure 4 owing to the finite number of emission sources that contribute to the 21cm signal. Given a beam radius  $\theta_{\text{beam}}$  and mass-averaged neutral fraction  $F_M$ , there are

$$N_{\text{cl}} \sim 400 \left( \frac{\theta_{\text{beam}}}{3.2'} \right)^2 \left( \frac{F_M}{0.03} \right) \left( \frac{M_c}{10^9 M_\odot} \right)^{-1} \times \left( \frac{\nu_{\text{bin}}}{5\text{MHz}} \right) \left( \frac{1+z}{7} \right)^{0.9} \quad (6)$$

emission sources within a frequency bin of width  $\nu_{\text{bin}}$  assuming the neutral clumps to have a *baryonic* mass  $M_c$ . Thus, we estimate that if the baryonic mass is limited to be the Jeans mass in an ionized IGM ( $M_c \sim 10^9 M_\odot$ ) then the component of uncertainty in a  $\nu_{\text{bin}} \sim 5\text{MHz}$  bin is around 5%, while the

existence of lower mass neutral clumps survived from the pre-reionization IGM would lead to an even smaller Poisson contribution. Of course a full calculation of  $N_{\text{cl}}$  would require a numerical simulation to resolve the details of the damped Ly $\alpha$  and Ly-limit systems. However equation (6) suggests that the finite distribution of neutral clumps will not contribute the dominant source of uncertainty in 21cm observations of quasar proximity zones with the MWA.

## 5 THE EFFECT OF FOREGROUND SUBTRACTION

The detection of a proximity zone will require the subtraction of a large foreground contribution to the redshifted 21cm signal. This foreground is thought to be dominated by synchrotron radiation, both galactic and extra galactic, and to be spectrally smooth (Oh & Mack 2003; Di Matteo et al. 2002). The processed band-pass of the MWA will be  $\Delta\nu = 32\text{MHz}$ , which corresponds to a physical length of  $\sim 50\text{Mpc}$  at  $z \sim 6$ . Thus the band pass that will be available to the MWA is similar in length to the profiles presented in Figure 4. The process of foreground subtraction will render any line-of-sight fluctuations with wavelengths comparable to, or larger than the band-pass undetectable. Thus, we expect to lose the overall trend of the emission with redshift across the band pass.

We take a simple approach to estimate the impact of foreground removal, fitting and subtracting a fourth order

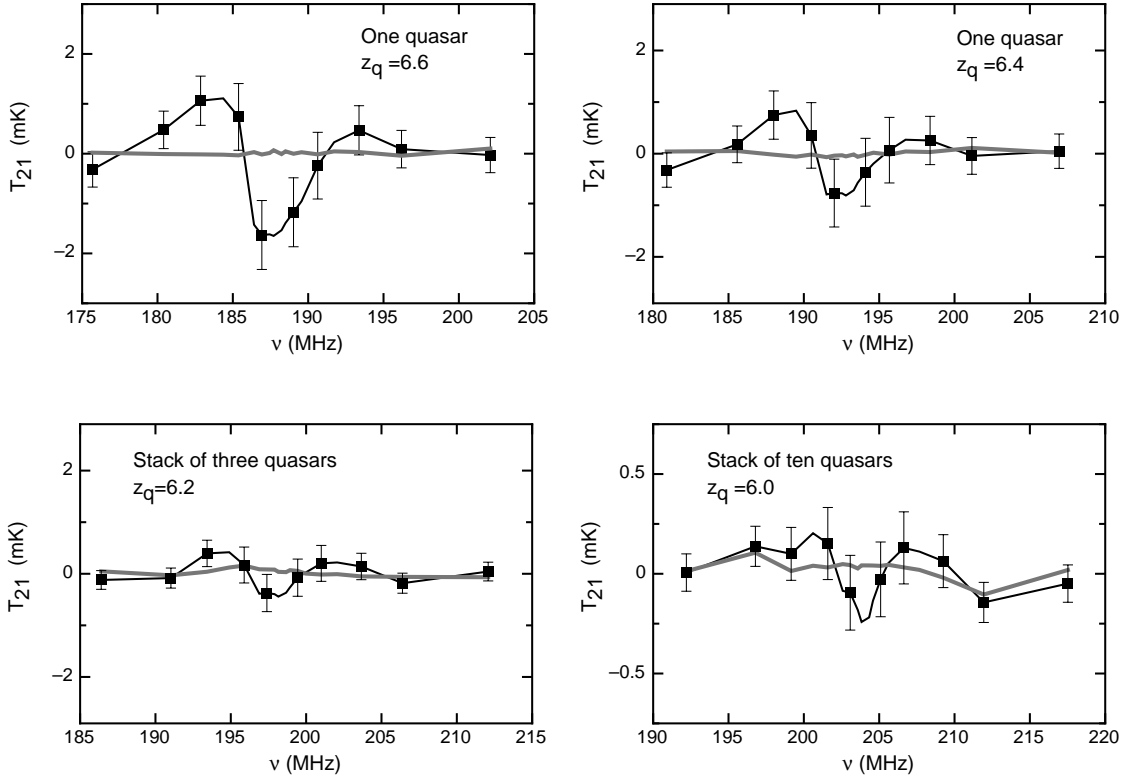


**Figure 5.** The 21cm brightness temperature as a function of observed frequency following subtraction of the best fit 4th order polynomial. The four panels show examples corresponding to the 4 different quasar redshifts described in Figure 4. Also shown are the corresponding examples for the mean IGM, centered on the assumed quasar redshifts (grey curves). At  $z \geq 6.2$ , the error bars shown correspond to an observation of 1000 hours with the MWA using a maximum baseline corresponding to a 3.2' beam. At  $z = 6.2$  and  $z = 6.0$  the errors assume an average signal from stacks of 3 and 10 quasars respectively.

polynomial from the model spectra in Figure 4. The resulting profiles are shown in Figure 5 (dark lines). We see that the subtraction removes the low order fluctuations, including the overall rise in intensity across the band-pass. However the subtraction leaves fluctuations around the slow rise due to the proximity zone. These fluctuations will be detectable, and their amplitude will yield the mass-averaged neutral fraction of hydrogen in the IGM at redshifts near that of the quasar. The asymmetry of the HII region, which is clear in Figure 4 would be difficult to detect in the foreground removed spectra shown in Figure 5. We will quantify this statement below.

In Figure 5 we also show the corresponding 21cm spectra for the mean IGM centered on the assumed quasar redshifts, with a fourth order polynomial fit subtracted as before. The resulting profiles are shown as the grey curves. These profiles have no detectable fluctuations. This is because the overlap epoch will take place over a range of redshifts that is larger than the frequency bandpass of the MWA. We therefore find that the global step will be undetectable by the MWA (or any instrument with a comparable bandpass). Note in this context that the modeling presented yields a global step that is as rapid as allowed in a standard cosmological scenario.

We next quantify the significance with which the quasar proximity zones could be detected in redshifted 21cm spectra. Our discussion is limited to determination of the confi-

dence with which the spectral feature at the redshift of the quasar (and its asymmetry, see Figure 4) could be detected. We define detection as the statistically significant rejection of a null-hypothesis comprised of the best fit 4th order polynomial to the spectra shown in Figure 4. Our approach is to compute a set of Monte-Carlo realisations of the 21cm spectrum by adding Gaussian noise to the model spectra shown in Figure 4. The Gaussian noise is assumed to have a distribution of variance equal to the noise shown in Figures 4-5. Using this set of noisy model spectra we construct the cumulative distribution of the confidence with which the HII region can be distinguished from a smooth (4th order polynomial) evolution in the 21cm signal. Specifically, we construct the cumulative distribution of the confidence  $C$ , defined as the probability that a value of  $\chi^2$  larger than observed would arise by chance given the null-hypothesis consisting of the best fit 4th order polynomial. The resulting distributions are plotted in the left hand panel of Figure 6, at four redshifts corresponding to the examples shown in Figures 4-5. As before we assume a noise level corresponding to a single quasar at  $z \geq 6.4$ , and stacks of 3 and 10 quasars at  $z = 6.2$  and  $z = 6$  respectively. Note that we have fitted spectra comprised of 10 points with a 5 parameter polynomial fit, leaving only 5 degrees of freedom. As a result any residuals left following subtraction of the fit lead to a high confidence for rejection of the null hypothesis. In these examples, the spectral dip could be detected with 90%



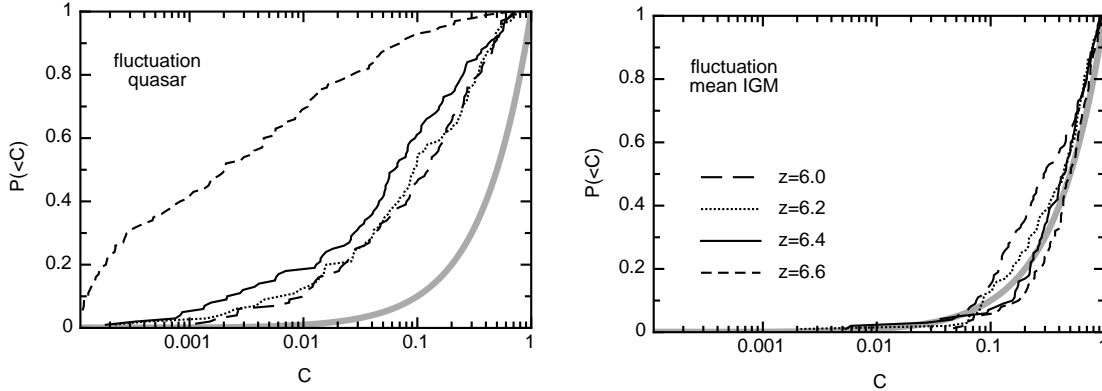


**Figure 6.** *Left panel:* Monte-Carlo realisations of the confidence with which the proximity zone can be distinguished from a smooth (modeled as a 4th order polynomial) evolution in the 21cm signal. Specifically, the quantity  $C$  is the probability that a value of  $\chi^2$  larger than that observed would arise by chance given a null-hypothesis consisting of the best fit 4th order polynomial. *Right panel:* The corresponding distributions for spectra of the mean IGM. In each case the plot shows the cumulative distribution of  $C$ , at 4 redshifts corresponding to the examples shown in Figures 4-5. Also shown for comparison is the cumulative probability distribution  $P_{\text{lin}}(< C) = C$  (thick grey lines).

confidence in 50% of cases for  $6.0 \lesssim z \lesssim 6.4$ . At  $z \sim 6.6$  the spectral feature would be detected with 99% confidence in more than 50% of cases.

In the right hand panel of Figure 6 we show the corresponding cumulative probability distributions for the confidence  $C$  of detecting a departure of the mean IGM spectrum from the 4th order polynomial best fit. In each case we show cumulative distributions for  $C$  computed from mean IGM spectra centered at four redshifts corresponding to the quasars in Figures 4-5. The probability of the observed spectrum being inconsistent (in a  $\chi^2$  sense) with the best fit 4th order polynomial is significantly less for the mean IGM spectrum than for the quasar spectra, indicating that the mean IGM signal is better modeled by a 4th order polynomial than a quasar near-zone.

For comparison, we also plot the cumulative distribution  $P_{\text{lin}}(< C) = C$  in both panels of Figure 6 (thick grey lines). In cases where the 4th order polynomial perfectly models the spectrum, we would expect no deviation of  $P(< C)$  from  $P_{\text{lin}}(< C)$ . Figure 6 therefore illustrates that the probability of a large value of  $\chi^2$  is well in excess of random for spectra of quasar near zones at all redshifts considered. On the other hand, for spectra of the mean IGM, we find that the three higher redshifts considered ( $z \geq 6.2$ ) have distributions  $P(< C)$  that are nearly indistinguishable from  $P_{\text{lin}}$ , as might be expected from the very smooth mean IGM spectra shown in Figure 4. At  $z = 6.0$  the 4th order polynomial does not adequately describe the spectrum at the end of overlap. As a result,  $P(< C) > P_{\text{lin}}(< C)$ . Nonetheless, as mentioned above,  $P(< C)$  is larger for the quasar spectrum than for the mean IGM spectrum for each of the four cases considered.

As noted earlier, the progression of overlap during the light travel time across the proximity zone leads to the asymmetric 21cm spectra shown in Figure 4. However following the subtraction of a 4th-order polynomial, the asymmetry is less pronounced. To quantify whether the asymmetry could be detected in the foreground removed spectra, we subtract the points in the foreground removed spectra at negative

$R$  from points at positive  $R$ . This produces curves of residual asymmetry  $\Delta T_{21}(R) = T_{21}(R) - T_{21}(-R)$  consisting of 5 points which are shown in Figure 7. Inspection of these residuals indicates that foreground removal will prohibit the detection of asymmetry, which would show up in Figure 7 as values of  $\Delta T_{21}$  that differ from zero. To quantify this statement, we compute the value of  $\chi^2$  relative to the null-hypothesis of a symmetric model (which would equal 0 at each  $R$ ). We compute this  $\chi^2$  and the associated confidence  $C$  for each of the Monte-Carlo model spectra assuming a  $\chi^2$  distribution with 5-2=3 degrees of freedom (corresponding to 5 points with comparison to a straight line). We then construct the cumulative probability distribution  $P(< C)$  as before. The resulting distributions are plotted in Figure 8, along with the cumulative probability distribution  $P_{\text{lin}}(< R) = C$  (thick grey lines). The left panel shows results for spectra of quasar proximity zones, while the right panel shows results for spectra of the mean IGM. The distributions indicate that asymmetry in the 21cm spectra of quasar near-zones could not be detected with high confidence under the observational conditions assumed in this paper.

## 6 LUMINOSITY FUNCTION AND NUMBER COUNTS OF HIGH REDSHIFT QUASARS

The advent of large multi-wavelength optical surveys in recent years has allowed the detailed study of the quasar luminosity function to be extended from redshifts corresponding to the peak of quasar activity ( $z \sim 3$ ), out to the end of the reionization era at  $z \gtrsim 6$ . Firstly, the density of quasars at a redshift of  $z \sim 6$  has been measured using the 8000 square degrees of imaging from the Sloan Digital Sky Survey (SDSS), yielding 21 quasars with  $z > 5.8$  and brighter than a  $z$ -band apparent AB-magnitude of  $m_z = 20$  (Fan et al. 2001; Fan et al. 2004; Fan et al. 2006). In addition, fainter  $z \sim 6$  quasars have been discovered in a deeper survey of the SDSS equatorial stripe (yielding 5 quasars over  $\sim 125$  square

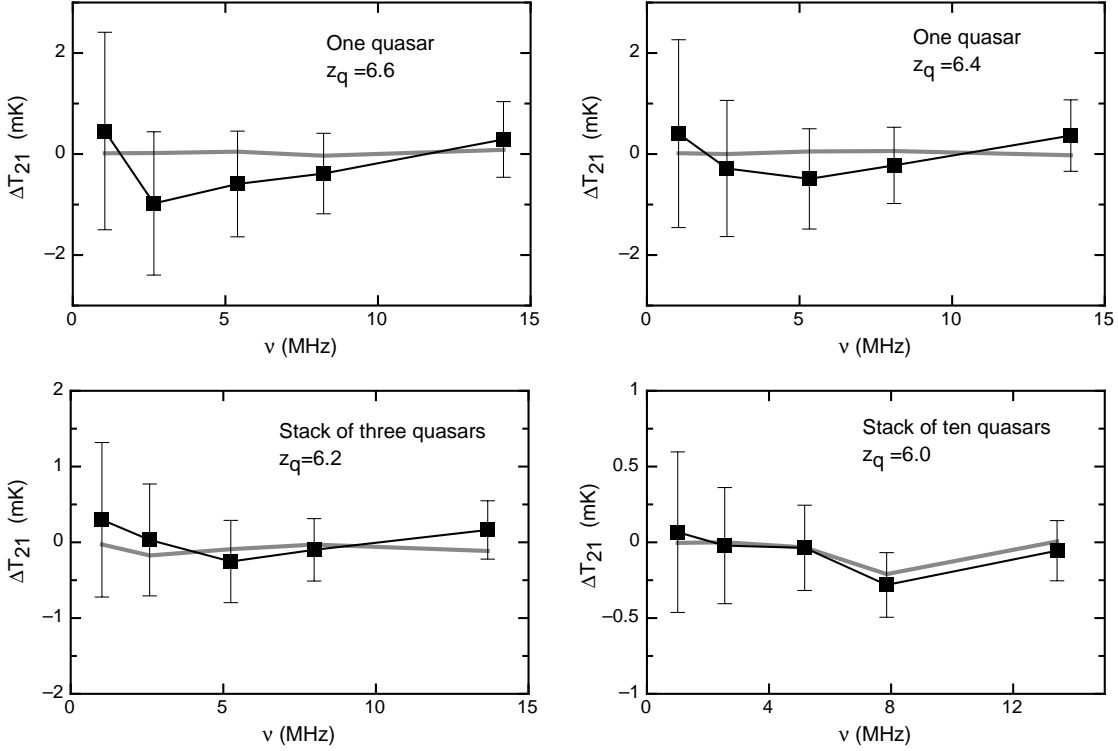


**Figure 7.** The difference ( $\Delta T_{21}$ ) between the 21cm brightness temperature in front and behind the quasar following subtraction of the best fit 4th order polynomial.  $\Delta T_{21}$  is plotted as a function of frequency difference relative to the quasar. A value of  $\Delta T_{21} = 0$  indicates a foreground removed spectrum that is symmetric about the quasar redshift. The four panels show examples corresponding to the 4 different quasar redshifts described in Figure 4. Also shown are the corresponding examples for the mean IGM, centered on the assumed quasar redshifts (grey curves). At  $z \geq 6.2$ , the error bars shown correspond to an observation of 1000 hours with the MWA using a maximum baseline corresponding to a  $3.2'$  beam. At  $z = 6.2$  and  $z = 6.0$  the errors assume the average signal from stacks of 3 and 10 quasars respectively.

degrees brighter than  $m_z = 21$ ; Jaing et al. 2007). The combination of deep and wide surveys has allowed the slope of the quasar luminosity function to be measured with high accuracy, and yields a space density of quasars at  $z \sim 6$  which may be parameterised using the form

$$\Theta_6(M_{1450}) = \Theta_6^* 10^{-0.4(\beta+1)(M_{1450}+26)}, \quad (7)$$

where  $\Theta_6^* = (5.2 \pm 1.9) \times 10^{-9} \text{Mpc}^{-3} \text{mag}^{-1}$ , and  $\beta = -3.1 \pm 0.4$  (Jiang et al. 2007). The corresponding integral version of the luminosity function is

$$\begin{aligned} \Psi_6(M_{1450}) &= \int_{-\infty}^{M_{1450}} \Theta_6(M_{1450}) dM_{1450} \\ &= \Psi_6^* 10^{-0.4(\beta+1)(M_{1450}+26)}, \end{aligned} \quad (8)$$

where

$$\Psi_6^* \equiv \frac{\Theta_6^*}{-0.4 \ln(10)(\beta+1)}. \quad (9)$$

Comparison of the space density of luminous quasars at  $z \sim 6$  (Fan et al. 2004) with the density measured at  $z \sim 4.3$  (Fan et al. 2001) shows an exponential decline in quasar number density with redshift

$$\Psi(M_{1450} < -26.7, z) \propto 10^{B \times z}, \quad (10)$$

where  $B = -0.49 \pm 0.07$  (Wyithe & Padmanabhan 2005).

The slope of the luminosity function ( $\beta$ ) changes between  $z \sim 4.3$  and  $z \sim 6$ , becoming steeper towards high redshift. However we will assume that  $\beta$  is constant at  $z \gtrsim 6$ , noting that since we are interested in extrapolation to quasars of lower luminosity than those already known, this will lead to conservative number counts. With the assumption of constant  $\beta$ , and following equation (10) we next write

$$\Theta^*(z) = \Theta_6^* \times 10^{B(z-6)}, \quad (11)$$

yielding the differential and cumulative luminosity functions

$$\Theta(M_{1450}, z) = \Theta_6^* \times 10^{B(z-6)} 10^{-0.4(\beta+1)(M_{1450}+26)}, \quad (12)$$

and

$$\Psi(M_{1450}, z) = \Psi_6^* \times 10^{B(z-6)} 10^{-0.4(\beta+1)(M_{1450}+26)}. \quad (13)$$

These estimates provide a strong empirical basis with which to predict the number counts of quasars at moderately larger redshifts, but with luminosities comparable to those currently observed.

## 7 ESTIMATED NUMBER COUNTS FOR FUTURE SURVEYS

Our goal in this section is to estimate the number of quasar proximity zones that might be available for study with low

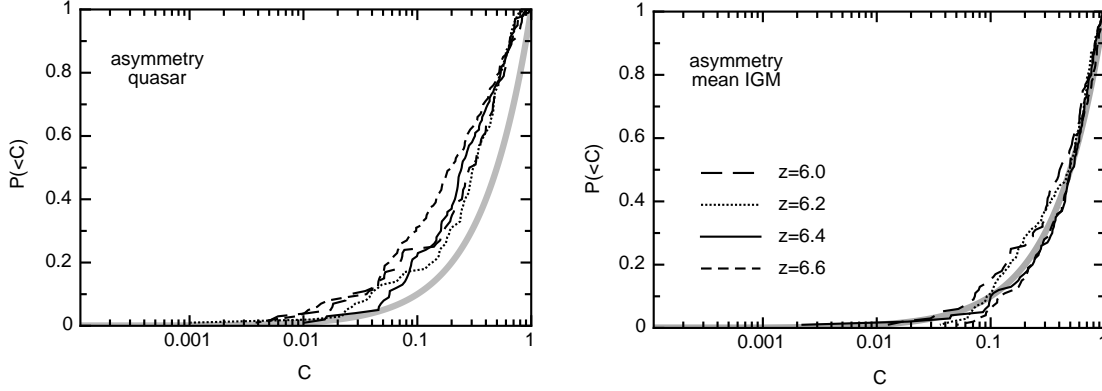


**Figure 8.** *Left panel:* Monte-Carlo realisations of the confidence with which asymmetry can be detected in the best fit foreground subtracted spectrum of a proximity zone. Specifically, the quantity  $C$  is the probability that a value of  $\chi^2$  larger than that observed would arise by chance given a null-hypothesis consisting of a symmetric proximity zone. *Right panel:* The corresponding distributions for spectra of the mean IGM. In each case the plot shows the cumulative distribution of  $C$ , at 4 redshifts corresponding to the examples shown in Figures 4-5. Also shown for comparison is the cumulative probability distribution  $P_{\text{in}}(<C) = C$  (thick grey lines).

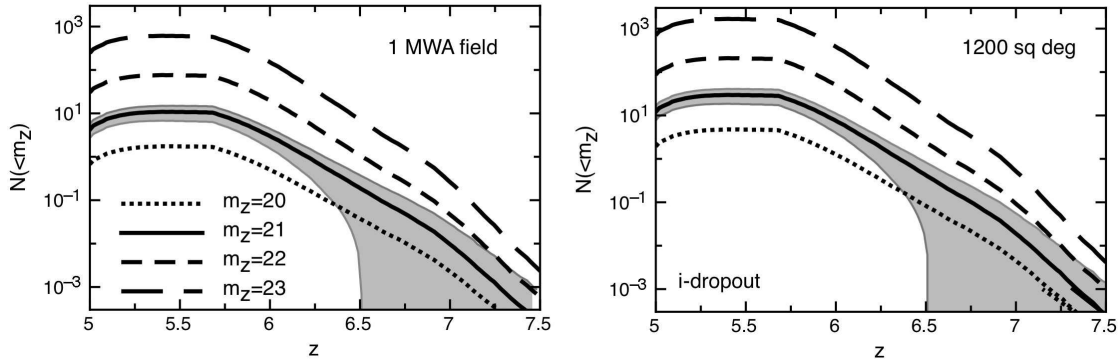


**Figure 9.** The number of quasars brighter than  $m_z$  within a 32MHz band whose high frequency end observes the 21cm line at redshift  $z$ . We plot estimates of the 1-sigma range for a limit  $m_z < 21$ . The left-hand and right-hand panels show the numbers for an MWA field, and a 1200 square degree area.

frequency arrays. As a specific example we consider the MWA, and multiply the density of quasars by the volume within an MWA observation in order to estimate the potential number counts. Using relations from Furlanetto, Oh & Briggs (2006), we obtain the co-moving volume of a cylinder of angular radius  $\theta$  and depth  $\Delta\nu$  around a frequency  $\nu$  corresponding to the 21cm line at redshift  $z$

$$V(\theta, \Delta\nu, z) = 4 \times 10^9 \left( \frac{\theta}{12\text{deg}} \right)^2 \left( \frac{1+z}{7} \right)^{0.9} \left( \frac{\Delta\nu}{32\text{MHz}} \right) \text{Mpc}^3. \quad (14)$$

Combining this volume with the quasar luminosity function we obtain the number counts of quasars per frequency interval  $\Delta\nu$  at a redshift  $z$  brighter than  $M_{1450}$

$$\begin{aligned} \frac{dN(M_{1450}, z)}{d\nu} \Delta\nu &= V(\theta, \Delta\nu, z) \Psi(<M_{1450}, z) \\ &= \frac{-\Theta_6^* \times 10^{10}}{\ln(10)(1+\beta)} 10^{-0.4(\beta+1)(M_{1450}+26)} \\ &\times \left( \frac{1+z}{7} \right)^{1.9} \left( \frac{\Delta\nu}{32\text{MHz}} \right) 10^{B(z-6)} \end{aligned} \quad (15)$$

Here we have noted that the field of view for the MWA is

$$\pi\theta^2 \sim \frac{\lambda^2}{(4m)^2} \times \frac{41253}{4\pi} \text{ square degrees}, \quad (16)$$

with  $\nu\lambda = c$  (yielding  $\theta = 12[(1+z)/7]$  degrees). Integrating over the redshift interval corresponding to the MWA bandpass of  $\Delta\nu = 32\text{MHz}$ , we find

$$N(M_{1450}, z) = \int_{\nu-\Delta\nu}^{\nu} \frac{d\nu}{\Delta\nu} \frac{dN(<M_{1450}, z)}{d\nu} \Delta\nu, \quad (17)$$

where the redshift  $z = 7(\nu/204.1\text{MHz}) - 1$  corresponds to the 21cm line redshifted to the high frequency end of the bandpass. We next convert these number counts for an absolute AB-magnitude  $M_{1450}$  to observed number counts for an apparent magnitude limit using the median spectrum from the LBQS (Francis et al. 1991), as well as the SDSS transmission curves for the  $i$  and  $z$ -filters. We assume that flux is fully absorbed in the Ly $\alpha$  forest below an observed wavelength  $1216(1+z)\text{\AA}$ , which is appropriate for  $z \gtrsim 5.8$  quasars (e.g. White, Becker, Fan, Strauss 2003).

We present number counts for one MWA field, and also for a 1200 square degree region. These are shown in Fig-

ure 9 as a function of redshift for four different  $z$ -band limiting AB-magnitudes. The counts are presented assuming  $\Delta\nu = 32\text{MHz}$  bandpass (which extends over a large fraction of a redshift unit). In Figure 9 the labeled redshift corresponds to the frequency of the redshifted 21cm line at the high frequency end of the observing band (see equation 17). As a concrete example, it is anticipated that the forthcoming Sky Mapper survey will reach  $i \sim 23$  in its six-epoch survey (Keller et al. 2007). Since  $z \sim 6$  quasars are discovered using an  $i$ -dropout criteria ( $i - z > 2.2$ ; Fan et al. 2001) the corresponding limiting magnitude achieved would be  $m_z \sim 21$ . This limit is shown as the solid line in Figure 9, along with the grey shaded region which refers to the 1-sigma uncertainty in the observed luminosity function. The  $i$ -dropout requirement limits discovery to  $z \gtrsim 5.75$ , which produces the plateau at lower redshifts. Our estimates suggest that at most one  $z > 6.5$  quasar ( $1\text{-}\sigma$  upper limit) will be discovered in a 1200 square degree region at  $m_z < 21$ , while one  $z > 6.25$  quasar would be found in each MWA field. At slightly lower redshifts the number counts will allow for stacking of signal from a number of quasars. For example, we would expect to find  $\sim 5$  quasars with  $z > 6$  per MWA field.

## 8 CONCLUSION

The introduction of low-frequency radio arrays over the coming decade is expected to revolutionize the study of the reionization epoch. Several studies have been published previously, arguing that the observation of the contrast in redshifted 21cm emission between a large HII region and the surrounding neutral IGM will be the simplest and most easily interpreted signature. These studies have focused on the detection of an HII region, formed by the ionizing flux from a quasar generating an ionized bubble in a significantly neutral IGM. However the highest redshift quasars so far discovered (at  $z \sim 6.4$ ) suggest that the IGM along those lines-of-sight is substantially ionized. Thus, more distant quasars would need to be discovered in order to find an HII region surrounding a previously known source. However quasars are observed to be extremely rare at high redshifts, and as discussed in § 7, the prospects for their discovery at  $z > 6.5$  in a region of around 1000 square degrees are not good. Alternatively the HII region might be found directly from 21cm data. While first generation instruments will detect an individual HII region at modest signal to noise, it has been suggested that a matched filter approach could be used to find HII regions in a blind search (Datta, Bharadwaj & Choudhury 2007). On the other hand, quasar HII regions will have a very complex geometry during the overlap epoch, even if they emit isotropically (Geil & Wyithe 2007), making the blind detection via a matched filter approach more difficult.

In this paper we have investigated the prospects for detection of proximity zones in the highly ionized IGM surrounding quasars during the late stages of the overlap era. We have concentrated on quasars at redshifts where they are already known to exist in sufficient numbers to make the measurements practical. We employ a semi-analytic model which reproduces several post overlap properties of the IGM, including the ionizing photon mean-free-path, the mass-averaged density of neutral gas and the hydrogen ionization

rate. In agreement with more sophisticated numerical simulations (e.g. Lidz et al. 2007; Bolton & Haehnelt 2007a), this model predicts that the Gunn-Peterson Trough will appear in the spectra of quasars at  $z \sim 6.4$ , even though the IGM is highly ionized by that time. We show that while quasars at  $z < 6.5$  are likely observed in the post overlap IGM, they will still provide valuable probes of the reionization era. This usefulness arises firstly because dense pockets of neutral gas will continue to provide a 21cm signal even in a highly ionized IGM. Secondly, the light-travel time across a quasar proximity zone is probably comparable to the duration of hydrogen overlap. As a result, while the IGM studied in Ly $\alpha$  absorption along the line-of-sight to the quasar may be highly ionized, the IGM observed "behind" the quasar would be in an earlier stage of overlap and so more neutral.

We have estimated the 21cm signal corresponding to quasar proximity zones as a function of distance from the quasar. At  $z \sim 6.4$  our model predicts that while the expected contrast in front of the quasar is less than  $\sim 1\text{mK}$ , at redshifts beyond the quasar the contrast would be as large as  $5\text{mK}$ . On the other hand, around a quasar at  $z \sim 6.0$  the contrast would be only  $\sim 0.5 - 1\text{mK}$ . Assuming observations using the configuration of the MWA, with 1000 hours of observing time and a maximum baseline corresponding to a  $3.2'$  beam we find that these contrasts could be detected in observations of individual quasars at  $z \gtrsim 6.4$ , while at  $z \leq 6.2$  detection would require a stack of observations for several quasars.

In practice the detection of a proximity zone will require the subtraction of the large foreground component which dominates the redshifted 21cm signal. The process of foreground subtraction will render any line-of-sight fluctuations with wavelengths comparable to, or larger than the bandpass undetectable. We therefore fit and subtract a fourth order polynomial to our model proximity zone spectra. We find that the subtraction removes the low order fluctuations including the overall rise across the band-pass. However the subtraction leaves residual fluctuations due to the proximity zone that would be detectable with the MWA, although the asymmetry of the proximity zone due to the evolution of the IGM will not. In contrast we find that foreground subtraction from the 21cm emission spectra corresponding to the mean IGM leaves no detectable fluctuations. This is because the overlap epoch will take place over a range of redshift that is larger than the frequency bandpass of the MWA. Foreground subtraction will render the global step in 21cm emission undetectable within a single  $\Delta\nu = 32\text{MHz}$  bandpass.

In our model we have used an analytic probability distribution for the over density which was fit to numerical simulations (Miralda-Escude et al. 2000). This model allows reionization to be computed in an inhomogeneous IGM, and provides a framework within which to model the progression of reionization from the era prior to overlap when the neutral gas is found predominantly in the mean IGM to post overlap where dense systems (DLAs) dominate the neutral hydrogen content of the universe (Prochaska et al. 2005). At redshifts lower than considered in this paper ( $z \lesssim 5$ ) observations of proximate DLAs (those within 3000 km/s of the observed quasar) show a density of neutral hydrogen that is comparable to the mean IGM (Prochaska et al. 2007). On the other hand, given the measured galaxy bias of DLAs, an excess of

DLAs would be expected in the over dense IGM where the proximate DLAs are observed. Prochaska et al. (2007) interpret this result as evidence that the quasar flux creates a proximity zone in the DLAs. Our model includes the mean enhancement of over density in the IGM surrounding the quasar but does not include a galaxy bias for the galaxies that are thought to host the DLAs at more intermediate redshifts. Thus, we expect the model to provide a qualitatively correct description prior to and during reionization. However at the lowest redshifts considered the unknown properties of DLAs could modify our model predictions.

The density of quasars at  $z \sim 6$  is now well constrained (Fan et al. 2006). We have employed the latest measurements of quasar densities at high redshift to estimate the number of quasars that will be discovered in optical–near-IR surveys, with specific reference to the numbers that may be found in MWA fields. Assuming that the MWA fields can be aligned with such surveys we estimate the number of quasars that will be discovered per MWA field. One particular example is the Sky Mapper survey (Keller et al. 2007), which will find around one quasar at  $z > 6.25$ , and around 5 quasars at  $z > 6$  per MWA field. Surveys for high redshift quasars (e.g. Sky Mapper) will cover a much larger fraction of the sky than is planned for redshifted 21cm observations. The fact that upcoming surveys will find more than 1  $z > 6$  quasar per MWA field is therefore important, since it means that redshifted 21cm observations do not need to be made in fields where quasars have been previously discovered.

In summary we find that if 21cm foregrounds can be subtracted to a level below the thermal noise the 21cm emission, then proximity zones around high redshift quasars will provide a probe of the very end of the overlap era. These 21cm proximity zones will provide a bridge between measurements of 21cm intensity fluctuations during the peak of the reionization era and studies of Ly $\alpha$  absorption following the completion of reionization, and so facilitate study of the entire evolution of the ionization state of the IGM.

**Acknowledgments** The research was supported by the Australian Research Council. The author acknowledges helpful conversations with Abraham Loeb, Paul Geil and James Bolton, and would like to thank an anonymous referee for suggestions which have improved this paper.

## REFERENCES

- Barkana, R., Loeb, A. 2001, *Phys. Rep.*, 349, 125  
 Barkana, R., & Loeb, A. 2005, *MNRAS*, 363, L36  
 Barkana, R., & Loeb, A. 2005, *ApJ*, 626, 1  
 Barkana, R., & Loeb, A. 2005, *ApJL*, 624, L65  
 Becker, G. D., Rauch, M., & Sargent, W. L. W. 2007, *ApJ*, 662, 72  
 Bolton, J. S., & Haehnelt, M. G. 2007a, *MNRAS*, 374, 493  
 Bolton, J. S., & Haehnelt, M. G. 2007b, submitted to *MNRAS*  
 Bond, J. R., Cole, S., Efstathiou, G., & Kaiser, N. 1991, *ApJ*, 379, 440  
 Chen H.-W., Prochaska J. X., Gnedin N. Y., 2007, *ApJL*, 667, L125  
 Datta, K. K., Bharadwaj, S., & Choudhury, T. R. 2007, *ArXiv Astrophysics e-prints*, arXiv:astro-ph/0703677  
 Dijkstra, M., Haiman, Z., Rees, M. J., & Weinberg, D. H. 2004, *ApJ*, 601, 666  
 Di Matteo, T., Perna, R., Abel, T., & Rees, M. J. 2002, *ApJ*, 564, 576  
 Efstathiou, G. 1992, *Mon. Not. R. Astron. Soc.*, 256, 43  
 Fan, X., et al. 2001, *AJ*, 121, 54  
 Fan, X., et al. 2004, *AJ*, 128, 515  
 Fan, X., et al. 2006, *AJ*, 132, 117  
 Francis, P. J., Hewett, P. C., Foltz, C. B., Chaffee, F. H., Weymann, R. J., & Morris, S. L. 1991, *ApJ*, 373, 465  
 Furlanetto, S. R., Zaldarriaga, M., & Hernquist, L. 2004, *ApJ*, 613, 16  
 Furlanetto, S. R., & Oh, S. P. 2005, *MNRAS*, 363, 1031  
 Furlanetto, S. R., Oh, S. P., & Briggs, F. H. 2006, *Phys. Rep.*, 433, 181  
 Geil, P. M., & Wyithe, S. 2007, *ArXiv e-prints*, 708, arXiv:0708.3716  
 Gnedin N. Y., 2007, *ArXiv e-prints*, 709  
 Gnedin, N. Y., & Fan, X. 2006, *ApJ*, 648, 1  
 Gnedin N. Y., Kravtsov A. V., Chen H.-W., 2007, *ArXiv e-prints*, 707  
 Gnedin, N. Y., & Shaver, P. A. 2004, *ApJ*, 608, 611  
 Jiang, L., et al. 2007, *ArXiv e-prints*, 708, arXiv:0708.2578  
 Keller, S. C., et al. 2007, *Publications of the Astronomical Society of Australia*, 24, 1  
 Kohler, K., Gnedin, N. Y., Miralda-Escudé, J., & Shaver, P. A. 2005, *ApJ*, 633, 552  
 Leitherer, C., et al. 1999, *ApJS*, 123, 3  
 Lidz, A., McQuinn, M., Zaldarriaga, M., Hernquist, L., & Dutta, S. 2007, *ArXiv Astrophysics e-prints*, arXiv:astro-ph/0703667  
 Loeb, A., & Zaldarriaga, M. 2004, *Physical Review Letters*, 92, 211301  
 Mesinger, A., Haiman, Z., & Cen, R. 2004, *ApJ*, 613, 23  
 Miralda-Escudé, J., Haehnelt, M., & Rees, M. J. 2000, *ApJ*, 530, 1  
 Nagamine, K., Wolfe, A. M., Hernquist, L., & Springel, V. 2007, *ApJ*, 660, 945  
 Oh, S. P., & Mack, K. J. 2003, *MNRAS*, 346, 871  
 Press, W., Schechter, P. 1974, *ApJ*, 187, 425  
 Prochaska, J. X., Herbert-Fort, S., & Wolfe, A. M. 2005, *ApJ*, 635, 123  
 Prochaska, J. X., Henawi, J. F., Herbert-Fort, S., 2007, *astro-ph/0703594*  
 Scott, J., Bechtold, J., Dobrzycki, A., & Kulkarni, V. P. 2000, *ApJS*, 130, 67  
 Shaver, P. A., Windhorst, R. A., Madau, P., & de Bruyn, A. G. 1999, *A&A*, 345, 380  
 Spergel, D. N., et al. 2007, *ApJS*, 170, 377  
 Srbinovsky, J. A., & Wyithe, J. S. B. 2007, *MNRAS*, 374, 627  
 Srbinovsky, J. A., & Wyithe, J. S. B. 2008, *MNRAS*, Submitted  
 Storrie-Lombardi, L. J., McMahon, R. G., Irwin, M. J., & Hazard, C. 1994, *ApJL*, 427, L13  
 Thoul, A. A., & Weinberg, D. H. 1996, *Astrophys. J.*, 465, 608  
 Tozzi, P., Madau, P., Meiksin, A., & Rees, M. J. 2000, *ApJ*, 528, 597  
 White, R., Becker, R., Fan, X., Strauss, M. 2003, *Astron J.*, 126, 1  
 Wyithe, J. S. B., Bolton, J. S., Haehnelt, M. 2007, *MNRAS*,

submitted

Wyithe, J. S. B, Loeb, A. 2003, ApJ, 586, 693

Wyithe, J.S.B, Loeb, A. 2004, Nature, 427, 815

Wyithe, J. S. B., & Loeb, A. 2004b, ApJ, 610, 117

Wyithe, S., & Loeb, A. 2007, ArXiv e-prints, 708,  
arXiv:0708.3392

Wyithe, J. S. B., Loeb, A., Barnes, D.G., 2005, ApJ, 634,  
715

Wyithe, J.S.B, Loeb, A., Carilli, C. 2005, ApJ, 628, 575

Wyithe, J. S. B., & Padmanabhan, T. 2006, MNRAS, 366,  
1029